Graphene in ultrafast and superstrong laser fields

Hamed Koochaki Kelardeh,[1] Vadym Apalkov,[1] and Mark I. Stockman[1,2,3]
[1]*Department of Physics and Astronomy, Georgia State University, Atlanta, Georgia 30303, USA*
[2]*Fakultät für Physik, Ludwig-Maximilians-Universität, Geschwister-Scholl-Platz 1, D-80539 München, Germany*
[3]*Max-Planck-Institut für Quantenoptik, Hans-Kopfermann-Strasse 1, D-85748 Garching, Germany*
(Received 26 September 2014; revised manuscript received 18 January 2015; published 30 January 2015)

For graphene interacting with a few-fs intense optical pulse, we predict unique and rich behavior dramatically different from three-dimensional solids. Quantum electron dynamics is shown to be coherent but highly nonadiabatic and effectively irreversible due to strong dephasing. Electron distribution in reciprocal space exhibits hot spots at the Dirac points and oscillations whose period is determined by nonlocality of electron response and whose number is proportional to the field amplitude. The optical pulse causes net charge transfer in the plane pf graphene in the direction of the instantaneous field maximum at relatively low fields and in the opposite direction at high fields. These phenomena promise ultrafast optoelectronic applications with petahertz bandwidth.

DOI: 10.1103/PhysRevB.91.045439 PACS number(s): 72.80.Vp, 05.60.Gg, 73.22.Pr, 78.47.J−

I. INTRODUCTION

Interactions of strong fields with solids have been studied from the onset of quantum mechanics [1–17]. Interest in this field has grown due to availability of ultrashort pulses with fields comparable to the internal fields in solids [6,10,18]. Such fields excite reversible electron dynamics and strongly modify properties of the solid within optical cycle, i.e., on the attosecond time scale [15–17]. Here we show theoretically that, in contrast, the strong-field interactions of graphene are highly nonadiabatic and irreversible causing significant electron transfer from the valence band resulting in high population of the conduction band, which persists after the pulse's end. These interactions result in ultrafast current whose density is orders of magnitude higher than that in dielectrics or metals [15,19]. Though graphene in the absence of an external field has a zero band gap (it is a semimetal), it does not necessarily mean that the corresponding electron dynamics is irreversible, since in an electric field electrons drift through the entire Brillouin zone, which introduces an effective band offset and a band gap ∼8 eV [20]. In this case, similar to dielectrics [16,17], one should have expected reversible dynamics. The extraordinary extreme nonlinear properties of graphene and the irreversibility in it are related to its unique electronic structure causing the singularity of the interband coupling in the vicinity of the Dirac points. It is this singularity that results in the irreversible electron dynamics in graphene.

We consider interaction of ultrashort laser pulses with graphene monolayer [21–23]. The purely two dimensional electron dynamics in graphene is characterized by unique dispersion relation, the low energy part of which is relativisticlike with linear dependence of the electron energy on momentum. The behavior of such low energy electrons is described by the Dirac relativistic massless equation. The Fermi energy of undoped graphene is at the Dirac point and, therefore, graphene is a semimetal with zero band gap. This should result in strong interband mixing of the valence band (VB) and the conduction band (CB). Below we consider femtosecond laser pulses whose duration τ_p is less than the electron scattering time ∼10–100 fs [24–29]. In this case, the electron dynamics is coherent and can be described by time-dependent Schrödinger equation.

In contrast, dynamics of graphene in relatively slow fields, $\tau_p \gtrsim 100$ fs, for which the scattering processes become important and the electron dynamics is incoherent, was studied [30] within the density matrix approach, where a hot-electron Fermi distribution was reported. For circularly polarized long optical pulses, interaction of electrons in graphene with periodic electric field results in formation of Floquet states and opening a gap in the energy spectrum [31–33] or graphenelike topological surface states of a topological insulator [34].

II. MODEL AND MAIN EQUATIONS

We consider an optical pulse that is incident normally on a graphene monolayer and parametrize it by the following single-oscillation form, which is an idealization of the actual 1.5-oscillation pulses used in recent experiments [15,16],

$$F(t) = F_0 e^{-u^2}(1 - 2u^2), \tag{1}$$

where F_0 is the amplitude, which is related to the pulse power $\mathcal{P} = cF_0^2/4\pi$, c is speed of light, $u = t/\tau$, and τ is the pulse length, which is set $\tau = 1$ fs corresponding to carrier frequency $\omega \approx 1.5$ eV$/\hbar$. Note that due to this parametrization, the pulse has always zero area, $\int_{-\infty}^{\infty} F(t)dt = 0$. We will assume that the pulse is linearly polarized, where the plane of polarization is characterized by angle θ measured relative to axis x. Here the x and y coordinate system is introduced in the plane of graphene and is determined by the crystallographic structure of graphene—see Fig. 1. The graphene has hexagonal lattice structure, which is shown in Fig. 1(a). The lattice has two sublattices, say "A" and "B," and is determined by two lattice vectors $\mathbf{a}_1 = a/2(\sqrt{3},1)$ and $\mathbf{a}_2 = a/2(\sqrt{3},-1)$, where $a = 2.46$ Å is the lattice constant. The distance between the nearest neighbor atoms of graphene is $a/\sqrt{3}$. The first Brillouin zone of the reciprocal lattice of graphene, which is a hexagon, is shown in Fig. 1(b). The points $K = (2\pi/a)(1/3,1/\sqrt{3})$ and $K' = (2\pi/a)(-1/3,1/\sqrt{3})$, which are the vertices of the hexagon, are the Dirac points. The energy gaps at these points are zero and the low energy spectra near these points are described by the Dirac relativistic equation. The points K and K' correspond to two valleys of low energy spectrum of graphene.

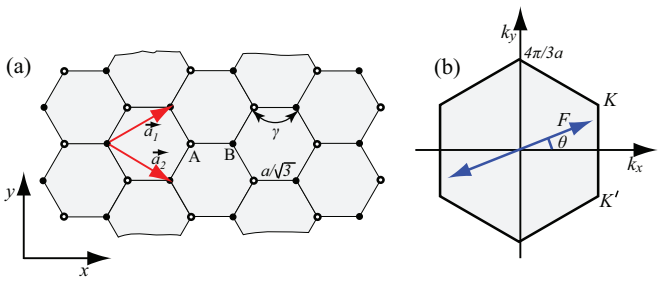

FIG. 1. (Color online) (a) Hexagonal lattice structure of 2D graphene. The graphene lattice consists of two inequivalent sublattices, which are labeled by "A" and "B." The vectors $\mathbf{a}_1 = a/2(\sqrt{3},1)$ and $\mathbf{a}_2 = a/2(\sqrt{3},-1)$ are the direct lattice vectors of graphene. The nearest-neighbor coupling, which is characterized by the hopping integral γ, is also shown. (b) The first Brillouin zone of reciprocal lattice of graphene. Points K and K' are two degenerate Dirac points, corresponding to two valleys of low energy spectrum of graphene. Blue line with arrows shows polarization of the time-dependent electric field of the pulse. The polarization is characterized by angle θ.

The Hamiltonian of electrons in graphene in the optical field has the form

$$\mathcal{H} = \mathcal{H}_0 + e\mathbf{F}(t)\mathbf{r}, \tag{2}$$

where $\mathcal{H}_0$ is the field-free electron Hamiltonian, $\mathbf{r} = (x,y)$ is a two-dimensional vector, and $\mathbf{F}(t) = [F(t)\cos\theta, F(t)\sin\theta]$. Below we consider the case of $\theta = 0$ only, i.e., pulse is polarized along the x axis. We consider a nearest-neighbor tight-binding model, which describes coupling between the two sublattices A and B of graphene with coupling constant $\gamma = -3.03$ eV [35–38]—see Fig. 1. In the reciprocal space the corresponding Hamiltonian $\mathcal{H}_0$ is a 2×2 matrix of the form [35,36]

$$\mathcal{H}_0 = \begin{pmatrix} 0 & \gamma f(\mathbf{k}) \\ \gamma f^*(\mathbf{k}) & 0 \end{pmatrix}, \tag{3}$$

where $\gamma = -3.03$ eV is the hopping integral and

$$f(\mathbf{k}) = \exp\left(i\frac{ak_x}{\sqrt{3}}\right) + 2\exp\left(-i\frac{ak_x}{2\sqrt{3}}\right)\cos\left(\frac{ak_y}{2}\right). \tag{4}$$

The energy spectrum of Hamiltonian $\mathcal{H}_0$ consists of conduction band (π^* or antibonding band) and valence bands (π or bonding band) with the energy dispersion $E_c(\mathbf{k}) = -\gamma|f(\mathbf{k})|$ (conduction band) and $E_v(\mathbf{k}) = \gamma|f(\mathbf{k})|$ (valence band). The corresponding wave functions are

$$\Psi^{(c)}_{\mathbf{k}}(\mathbf{r}) = \frac{e^{i\mathbf{k}\cdot\mathbf{r}}}{\sqrt{2}}\begin{pmatrix} 1 \\ e^{-i\phi_k}\end{pmatrix} \tag{5}$$

and

$$\Psi^{(v)}_{\mathbf{k}}(\mathbf{r}) = \frac{e^{i\mathbf{k}\cdot\mathbf{r}}}{\sqrt{2}}\begin{pmatrix} -1 \\ e^{-i\phi_k}\end{pmatrix}, \tag{6}$$

where $f(\mathbf{k}) = |f(\mathbf{k})|e^{i\phi_k}$. The wave functions $\Psi^{(c)}_{\mathbf{k}}$ and $\Psi^{(v)}_{\mathbf{k}}$ have two components belonging to sublattices A and B, respectively.

When the duration of the laser pulse is less than the characteristic electron scattering time, which is ~10–100 fs [24–29], the electron dynamics in external electric field of the optical pulse is coherent and can be described by the time-dependent Schrödinger equation

$$i\hbar\frac{d\Psi}{dt} = \mathcal{H}\Psi, \tag{7}$$

where the Hamiltonian (2) has explicit time dependence.

The electric field of the optical pulse generates both interband and intraband electron dynamics. The interband dynamics introduces a coupling of the states of the conduction and valence bands and results in redistribution of electrons between two bands. For dielectrics, such dynamics results in its metallization, which manifest itself as a finite charge transfer through dielectrics and finite conduction band population after the pulse ends.

It is convenient to describe the intraband dynamics, i.e., the electron dynamics within a single band, in the reciprocal space. In the reciprocal space, the electron dynamics is described by acceleration theorem, which has the following form:

$$\hbar\frac{d\mathbf{k}}{dt} = e\mathbf{F}(t). \tag{8}$$

The acceleration theorem is universal and does not depend on the dispersion law. Therefore, the intraband electron dynamics is the same for both conduction and valence bands. For an electron with initial momentum $\mathbf{q}$ the electron dynamics is described by the time-dependent wave vector, $\mathbf{k}_T(\mathbf{q},t)$, which is given by the solution of Eq. (8),

$$\mathbf{k}_T(\mathbf{q},t) = \mathbf{q} + \frac{e}{\hbar}\int_{-\infty}^{t}\mathbf{F}(t_1)dt_1. \tag{9}$$

The corresponding wave functions are the Houston functions [39], $\Phi^{(H)}_{\alpha q}(\mathbf{r},t)$,

$$\Phi^{(H)}_{\alpha\mathbf{q}}(\mathbf{r},t) = \Psi^{(\alpha)}_{\mathbf{k}_T(\mathbf{q},t)}(\mathbf{r})e^{-\frac{i}{\hbar}\int_{-\infty}^{t}dt_1 E_\alpha[\mathbf{k}_T(\mathbf{q},t_1)]}, \tag{10}$$

where $\alpha = v$ (valence band) or $\alpha = c$ (conduction band).

Using the Houston functions as the basis, we express the general solution of the time-dependent Schrödinger equation (7) in the following form:

$$\Psi_{\mathbf{q}}(\mathbf{r},t) = \sum_{\alpha=v,c}\beta_{\alpha\mathbf{q}}(t)\Phi^{(H)}_{\alpha\mathbf{q}}(\mathbf{r},t). \tag{11}$$

The solution (11) is parametrized by initial electron wave vector $\mathbf{q}$. Due to universal electron dynamics in the reciprocal space, the states, which belong to different bands (conduction and valence bands) and which have the same initial wave vector $\mathbf{q}$, will have the same wave vector $\mathbf{k}_T(\mathbf{q},t)$ at later moment of time t. Since the interband dipole matrix element, which determines the coupling of the conduction and valence band states in external electric field, is diagonal in the reciprocal space, then the states with different initial wave vectors are not coupled by the pulse field. As a result in Eq. (11), for each value of initial wave vector q, we need to find only two time-dependent expansion coefficients $\beta_{v\mathbf{q}}(t)$ and $\beta_{c\mathbf{q}}(t)$. Such decoupling of the states with different values of $\mathbf{q}$ is the property of coherent dynamics. For incoherent dynamics, the electron scattering couples the states with different wave vectors $\mathbf{q}$. In this case the dynamics is described by the density matrix.

The expansion coefficients satisfy the following system of differential equations:

$$\frac{d\beta_{c\mathbf{q}}(t)}{dt} = -i\frac{\mathbf{F}(t)\mathbf{Q}_{\mathbf{q}}(t)}{\hbar}\beta_{v\mathbf{q}}(t), \tag{12}$$

$$\frac{d\beta_{v\mathbf{q}}(t)}{dt} = -i\frac{\mathbf{F}(t)\mathbf{Q}^{*}_{\mathbf{q}}(t)}{\hbar}\beta_{c\mathbf{q}}(t), \tag{13}$$

where the vector-function $\mathbf{Q}_{\mathbf{q}}(t)$ is proportional to the interband dipole matrix element

$$\mathbf{Q}_{\mathbf{q}}(t) = \mathbf{D}[\mathbf{k}_T(\mathbf{q},t)]e^{-\frac{i}{\hbar}\int_{-\infty}^{t} dt_1\{E_c[\mathbf{k}_T(\mathbf{q},t_1)]-E_v[\mathbf{k}_T(\mathbf{q},t_1)]\}}, \tag{14}$$

where $\mathbf{D}(\mathbf{k}) = [D_x(\mathbf{k}), D_y(\mathbf{k})]$ is the dipole matrix element between the states of the conduction and valence bands with wave vector $\mathbf{k}$, i.e.,

$$\mathbf{D}(\mathbf{k}) = \left\langle \Psi^{(c)}_{\mathbf{k}} \middle| e\mathbf{r} \middle| \Psi^{(v)}_{\mathbf{k}} \right\rangle. \tag{15}$$

Substituting the conduction and valence band wave functions (5) and (5) into Eq. (15), we obtain the following expressions for the interband dipole matrix elements:

$$D_x(\mathbf{k}) = \frac{ea}{2\sqrt{3}}\frac{1+\cos\left(\frac{ak_y}{2}\right)\left[\cos\left(\frac{3ak_x}{2\sqrt{3}}\right)-2\cos\left(\frac{ak_y}{2}\right)\right]}{1+4\cos\left(\frac{ak_y}{2}\right)\left[\cos\left(\frac{3ak_x}{2\sqrt{3}}\right)+\cos\left(\frac{ak_y}{2}\right)\right]} \tag{16}$$

and

$$D_y(\mathbf{k}) = \frac{ea}{2}\frac{\sin\left(\frac{ak_y}{2}\right)\sin\left(\frac{3ak_x}{2\sqrt{3}}\right)}{1+4\cos\left(\frac{ak_y}{2}\right)\left[\cos\left(\frac{3ak_x}{2\sqrt{3}}\right)+\cos\left(\frac{ak_y}{2}\right)\right]}. \tag{17}$$

The system of equations (12) and (13) describes the interband electron dynamics and determines the mixing of the conduction band and the valence band states in the electric field of the pulse. There are two solutions of the system (12) and (13), which correspond to two initial conditions: $(\beta_{v\mathbf{q}},\beta_{c\mathbf{q}}) = (1,0)$ and $(\beta_{v\mathbf{q}},\beta_{c\mathbf{q}}) = (0,1)$. These solutions determine the evolution of the states, which are initially in the valence band or in the conduction band, respectively.

For undoped graphene all states of the valence band are occupied and all states of the conduction band are empty. For an electron, which is initially in the valence band the mixing of the states of different bands is characterized by the time-dependent component $|\beta_{c\mathbf{q}}(t)|^2$. We can also define the time-dependent total occupation of the conduction band for undoped graphene from the following expression:

$$\mathcal{N}_{CB}(t) = \sum_{\mathbf{q}} |\beta_{c\mathbf{q}}(t)|^2, \tag{18}$$

where the sum is over the first Brillouin zone and the solution $\beta_{c\mathbf{q}}(t)$ in Eq. (18) satisfies the initial condition $(\beta_{v\mathbf{q}},\beta_{c\mathbf{q}}) = (1,0)$.

Redistribution of electrons between the conduction and the valence bands in time-dependent electric field also generates electric current, which can be calculated in terms of the operator of velocity from the following expression:

$$J_j(t) = \frac{e}{a^2}\sum_{\mathbf{q}}\sum_{\alpha_1=v,c}\sum_{\alpha_2=v,c}\beta^{*}_{\alpha_1\mathbf{q}}(t)\mathcal{V}^{\alpha_1\alpha_2}_{j}\beta_{\alpha_2\mathbf{q}}(t), \tag{19}$$

where $j = x,y$ and $\mathcal{V}^{\alpha_1\alpha_2}_{j}$ are the matrix elements of the velocity operator $\hat{\mathcal{V}}_j = \frac{1}{\hbar}\frac{\partial\mathcal{H}_0}{\partial k_j}$ between the conduction and valence band states. With the known wave functions (5) and (6) of the conduction and valence bands the matrix elements of the velocity operator are

$$\mathcal{V}^{cc}_{x} = -\mathcal{V}^{vv}_{x} = \frac{a\gamma}{\sqrt{3}\hbar}\left[\sin\left(\frac{ak_x}{\sqrt{3}}-\phi_{\mathbf{k}}\right) + \sin\left(\frac{ak_x}{\sqrt{3}}+\phi_{\mathbf{k}}\right)\cos\frac{ak_y}{2}\right], \tag{20}$$

$$\mathcal{V}^{cc}_{y} = -\mathcal{V}^{vv}_{y} = \frac{a\gamma}{\hbar}\cos\left(\frac{ak_x}{2\sqrt{3}}+\phi_{\mathbf{k}}\right)\sin\frac{ak_y}{2}, \tag{21}$$

$$\mathcal{V}^{cv}_{x} = -i\frac{2a\gamma}{\sqrt{3}\hbar}\left[\cos\left(\frac{ak_x}{\sqrt{3}}-\phi_{\mathbf{k}}\right) - \cos\left(\frac{ak_x}{\sqrt{3}}+\phi_{\mathbf{k}}\right)\cos\frac{ak_y}{2}\right], \tag{22}$$

and

$$\mathcal{V}^{cv}_{y} = -i\frac{2a\gamma}{\hbar}\sin\left(\frac{ak_x}{\sqrt{3}}+\phi_{\mathbf{k}}\right)\cos\frac{ak_y}{2}. \tag{23}$$

The interband matrix elements of the velocity operator, $\mathcal{V}^{cv}_{x}$ and $\mathcal{V}^{cv}_{y}$, are related to the interband dipole matrix elements, $\mathcal{V}^{cv}_{x} = iD_x(\mathbf{k})[E_c(\mathbf{k}) - E_v(\mathbf{k})]/\hbar$ and $\mathcal{V}^{cv}_{y} = iD_y(\mathbf{k})[E_c(\mathbf{k}) - E_v(\mathbf{k})]/\hbar$ [40].

Within the nearest-neighbor tight-binding model, the graphene has electron-hole symmetry, which results in the relation $\mathcal{V}^{cc}_{y} = -\mathcal{V}^{vv}_{y}$. Inclusion into the model the higher order tight-binding couplings, e.g., next-nearest-neighbor terms, introduced electron-hole asymmetry, which results in different magnitudes of velocity in the conduction and valence bands [41]. This asymmetry is weak and does not change the main results presented below.

If the direction of electric field of the pulse is along the direction of high symmetry of graphene crystal, then the current (19) is generated along the direction of electric field of the pulse only, $J_{||}$. For graphene, the directions of high symmetry correspond to polarization angles $\theta = 0$ and 30°. If polarization of electric field is not along the direction of high symmetry of graphene, then the current is generated in both the direction of the field, $J_{||}$, and in the direction perpendicular to the field, $J_{\perp}$. Our results show that the perpendicular component of the current is more than two orders of magnitude smaller than the parallel component of the current. Therefore, we calculate only the parallel component of the current.

The generated current results in charge transfer through the system, which is determined by an expression

$$Q_{tr} = \int_{-\infty}^{\infty} dt\, J_{||}(t). \tag{24}$$

The transferred charge is nonzero only due to irreversibility of electron dynamics in the optical pulse. For completely reversible dynamics, when the system returns to its initial state, the transferred charge is exactly zero. Indeed, since the current can be expressed in terms of polarization $\mathbf{P}(t)$ of the electron system as $\mathbf{J}(t) = d\mathbf{P}(t)/dt$, then the transferred charge is determined by the residual polarization of the system,

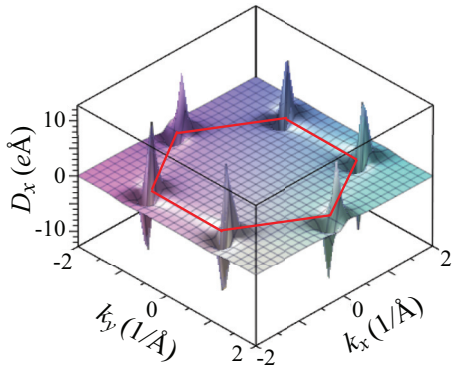

FIG. 2. (Color online) Interband dipole matrix element D_x is shown as a function of the wave vector $\mathbf{k}$. The red lines show the boundary of the first Brillouin zone. The dipole matrix element is singular near the Dirac points (K and K' points).

i.e., polarization of the electron system after the pulse ends, $Q_{tr} = P(t \to \infty)$. The residual population is nonzero only for irreversible dynamics.

III. RESULTS AND DISCUSSION

A. Conduction band population

Electron dynamics in an optical field is determined by two interrelated properties of graphene: (i) zero band gap, which results in strong interband mixing even in a weak electric field, and (ii) strong dependence of interband dipole matrix elements on the wave vector. These matrix elements, D_x and D_y, are singular at the Dirac points, K and K', as $\propto 1/\Delta k$, where $\Delta k = |k - k_K|$ is the distance in the reciprocal space from nearest Dirac point; see Fig. 2 (calculated in SI). Away from the Dirac points, $D_x \sim D_y \sim ea/2 \approx 1.2e$ Å. At the center of the Brillouin zone (the Γ point), $D_x = D_y = 0$. Thus there is strong interband coupling at the Dirac points and no coupling at the Γ point.

A strong optical electric field causes redistribution of electrons between the CB and the VB. The total CB population, $\mathcal{N}_{CB}(t)$ [see Eq. (18)]. It is displayed as a function of time t together with the corresponding time-dependent electric field, $F(t)$, in Fig. 3(a). Its qualitative features are in sharp contrast with those of dielectrics [16,42]. First, the electron kinetics is dramatically irreversible: when the pulse is over, the CB population does not return to zero staying at a high residual level $\mathcal{N}_{CB}^{(res)}$ which is close to the maximum CB population during the pulse, $\mathcal{N}_{CB}^{(max)}$. The second, related feature is that there is $a \sim \pi/2$ phase shift between $\mathcal{N}_{CB}(t)$ and the electric field, $F(t)$: the maximums of the conduction band population occur at zeros of the electric field. In contrast, for dielectrics, the CB population adiabatically follows the field, and their maximums coincide with a good accuracy [16,42].

Such irreversible electron dynamics takes place for all pulse amplitudes F_0 as Fig. 3(b) clearly demonstrates. The maximum CB population is reached at $t \approx 1$ fs; the residual (at the end of the pulse) CB population, $\mathcal{N}_{CB}^{(res)}$, is close to $\mathcal{N}_{CB}^{(max)}$ in all cases [Fig. 3(c)]. We have found (not shown) that the CB population has only a weak dependence on the polarization direction, and the results similar to Fig. 3 are obtained for other polarizations.

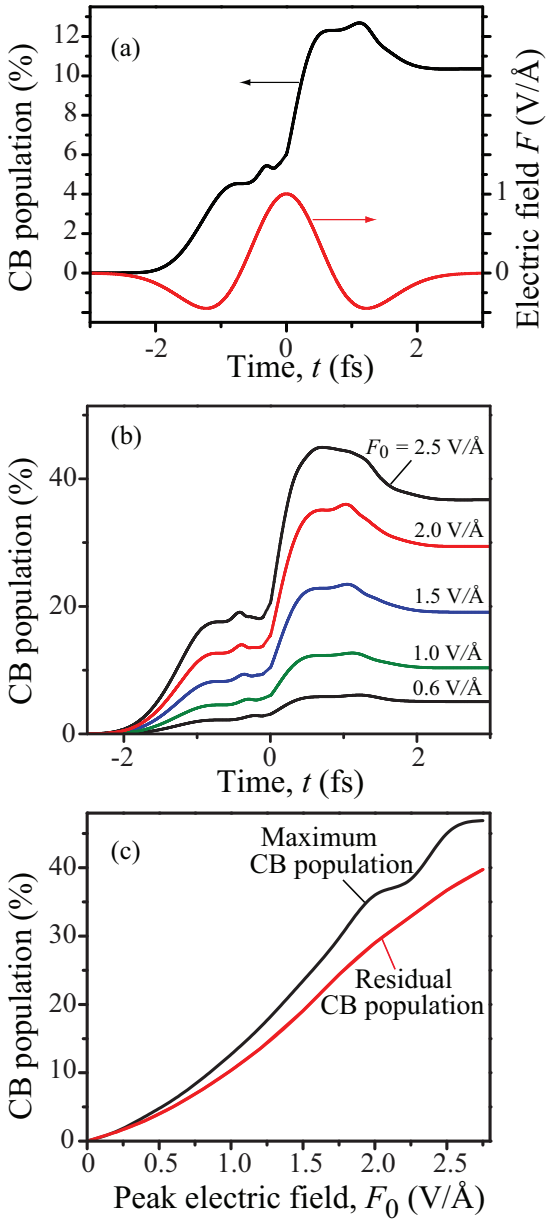

FIG. 3. (Color online) Population of the CB. (a) The CB population, $\mathcal{N}_{CB}(t)$, and the corresponding electric field, $F(t)$, of the laser pulse are shown as function of time t. The polarization of the pulse is along axis x, i.e., $\theta = 0$. (b) Series of the CB populations are plotted as functions of time for peak fields indicated on the graph. (c) The maximum and residual CB populations as functions of the peak electric field.

As we interpret, the irreversible electron dynamics is due to the gapless energy dispersion in graphene and strong dependence of the interband dipole matrix elements, D_x and D_y, on the wave vector. This causes a unique dependence of the Zener tunneling rate, $\Delta_l \propto l^{-1}$, where l is the number of unit cells through which the electron tunnels to cross the band gap [20]; in a sharp contrast, in 3D crystals, this dependence on l is exponential. This weak l dependence brings about strong resonance transitions between the VB and CB leading

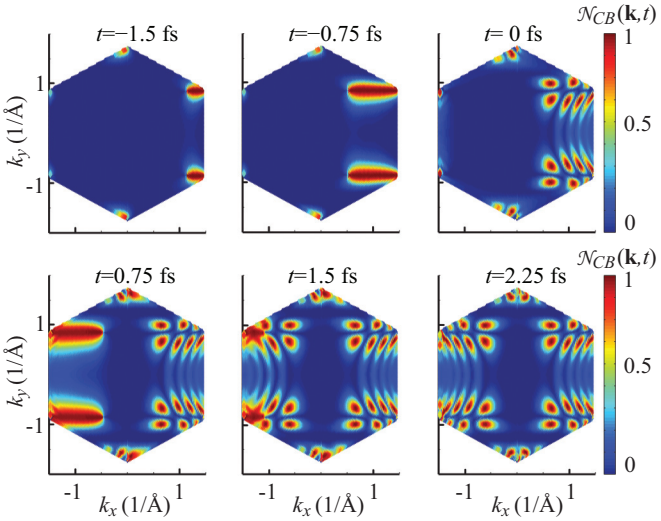

FIG. 4. (Color online) Conduction band population $\mathcal{N}_{CB}(\mathbf{k},t) = |\beta_{c\mathbf{k}}(t)|^2$ (see SI for definition) as a function of the wave vector at different moments of time. Only the first Brillouin zone of the reciprocal space is shown. The peak electric field of the pulse is $F_0 = 1$ V/Å. Different colors correspond to different values of the conduction band population as shown in the figure.

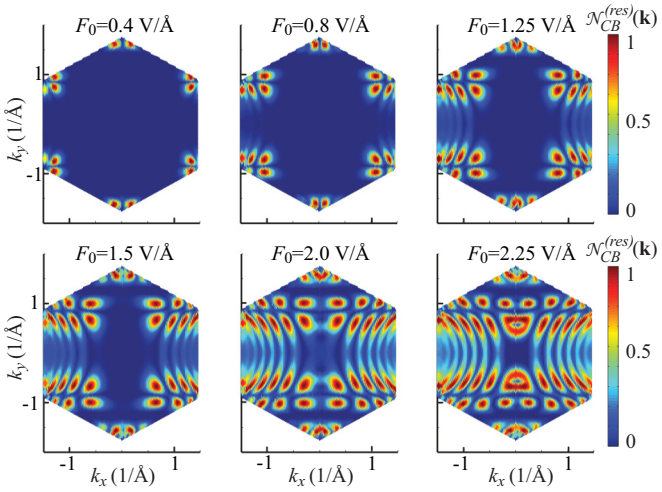

FIG. 5. (Color online) Residual conduction band population $\mathcal{N}_{CB}^{(res)}(\mathbf{k})$ as a function of wave vector $\mathbf{k}$ for different amplitudes F_0 of the optical pulse, as indicated. Only the first Brillouin zone is shown. The polarization of electric field is along axis x.

to dephasing (Landau damping), which effectively causes irreversibility for our time intervals.

The singularities of the dipole matrix elements at the Dirac points also result in a highly nonuniform distribution of the conduction band population in the reciprocal space, $\mathcal{N}_{CB}(\mathbf{k},t) = |\beta_{c\mathbf{k}}(t)|^2$ (see SI for definition), which is shown in Fig. 4. This population dynamics is unusual and dramatic. The electrons are accelerated by the field along its polarization direction (x axis) as determined by the time-dependent wave vector $\mathbf{k}(t)$ (see the acceleration theorem in SI),

$$\mathbf{k}(t) = \frac{e}{\hbar}\int \mathbf{F}(t)dt. \tag{25}$$

Initially, for $t < -0.75$ fs, the field is negative which accelerates the electrons to the right in Fig. 4. At the Dirac points due to the singular and large interband dipoles, the electrons are transferred VB $\rightarrow$ CB, which shows as two "jets" of high electron population at $k_x \approx 1$ Å^{-1}—see panels for $t = -1.5, -0.75$ fs. Then the field changes its sign, and the electrons start to move left and also undergo further VB $\rightarrow$ CB transitions leading to the appearance of the jets at $k_x \approx -1$ Å^{-1} and interference fringes at the $k_x \approx 1$ Å^{-1} Dirac points for $t \geqslant 0.75$ fs. Further, additional electrons are transferred causing the interference fringes at the $k_x \approx -1$ Å^{-1} Dirac points for $t = 1.5$ fs. The distribution becomes completely symmetric at the end of the pulse ($t = 2.25$ fs), which is a consequence of the zero pulse area.

Residual (after the pulse end) distributions $\mathcal{N}_{CB}^{(res)}(\mathbf{k})$ of the CB electrons in the reciprocal space for various field amplitudes F_0 are displayed in Fig. 5. They exhibit the jets at the Dirac points extended in the direction of the external field, which are modulated by the interference fringes. The extension, Δk, of the jets increases approximately proportionally to the field; it is defined by the acceleration in the average field during half-period: $\Delta k \sim eF_0/\omega$. For instance, for $F_0 = 1.5$ V/Å, $\Delta k \sim 1$ Å^{-1}, in agreement with Fig. 5. The spacing between the interference fringes, δk, is reciprocal to the nonlocality scale, i.e., the length electron displaces during the optical cycle, $\delta k \sim \omega/v_F \sim 0.2$ Å^{-1}, where $v_F \sim 10^8$ cm/s is the Fermi velocity; this estimate is also in agreement with Fig. 5.

The residual distribution of Fig. 5 shows the fringes with very high contrast: the maximum population probability, $\mathcal{N}_{CB}^{(res)}(\mathbf{k}) \approx 1$, and practically zero minimum population probability. Note that these fringes are created by a femtosecond pulse but can be relatively long lived, decaying with electron collision time τ.

At low excitation frequencies, we can estimate this time for doped graphene with equilibrium CB electron density n as $\tau = \hbar\mu\sqrt{\pi n}/(ev_F)$, where μ is the electron mobility. Setting $\mu \approx 2.5 \times 10^4$ cm^{2}V^{-1}s^{-1} at $n \approx 5 \times 10^{12}$ cm^{-2} [43,44] and $v_F = 1.15 \times 10^8$ cm/s [45], we obtain $\tau \approx 0.6$ ps. In contrast, at optical excitation frequencies and high intensities, time τ is reduced and is measured to be $\tau \sim 140$ fs [25]; for very high excitation densities, carrier multiplication processes become important, further reducing τ to a few tens of femtoseconds [27]. Electron-phonon processes are relatively slow, with scattering time $\tau \gtrsim 600$ fs [27]. Even the fastest electron collisions, with tens of femtosecond time, are much slower than the subcycle dynamics of $\lesssim$1 fs duration predicted in this article. The femtosecond and attosecond momentum imaging [17,46] is potentially capable of measuring the ultrafast transient dynamics predicted by Fig. 4.

The formation of the localized regions with high conduction band population, which is illustrated in Figs. 4 and 5 of the paper, is due to singularity of the intraband dipole matrix elements at the Dirac points. The interband dipole matrix elements are large near the Dirac points and are diverging exactly at the Dirac points. An electron with initial wave vector $\mathbf{q}$ propagates in the reciprocal space along the direction

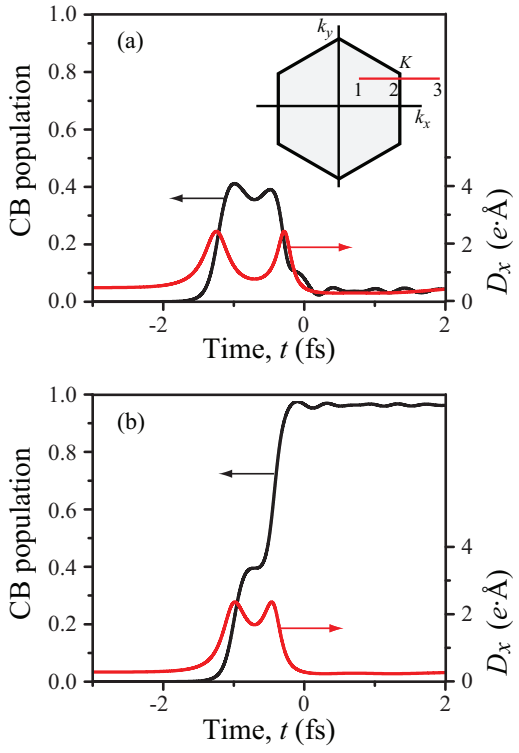

FIG. 6. (Color online) Time-dependent conduction band population and corresponding dipole matrix element D_x. The data are shown for a state with initial wave vector $\mathbf{q}$ of the reciprocal space. The conduction band population is calculated as $|\beta_{c\mathbf{q}}(t)|^2$ and the dipole matrix element is defined as $D_x(\mathbf{k}_T(\mathbf{q},t)$. Two different initial wave vectors in panels (a) and (b) correspond to small and large residual conduction band populations, respectively. The inset in panel (a) illustrates schematically the electron dynamics in the reciprocal space: the electron is transferred along the path "1"→"2"→"3"→"2"→"1". The polarization of the optical pulse is along axis x.

of electric field and the electron wave vector at a moment of time t is given by the function $\mathbf{k}_T(\mathbf{q},t)$; see Eq. (9). The trajectory of such an electron is shown schematically in the inset in Fig. 6(a), where the electron, which is initially at point "1", is transferred along the path "1"→"2"→"3"→"2"→"1" during the pulse. Since the area under the pulse is zero, the electron returns to its initial point "1". Along this closed path the interband coupling, which is proportional to the interband dipole matrix element, is the strongest near the point "2", closest to the Dirac points. Thus the strongest mixing of the CB and VB states occurs when the electron passes through point "2". For the closed path "1"→"3"→"1" there are two passages of point "2". As a result there are two strong changes in CB population. These two changes can be constructive or destructive, resulting in final large or small CB population, respectively. These two possibilities are shown in Fig. 6, where the time-dependent CB population is shown for two initial wave vectors $\mathbf{q}$. The time-dependent interband dipole matrix element, D_x, calculated at wave vector $\mathbf{k}_T(\mathbf{q},t)$, is also shown in Fig. 6. The two maxima in the time-dependent dipole matrix element correspond to two passages of the point "2" shown in the inset in Fig. 6(a). For both initial wave vectors [see Figs. 6(a) and 6(b)] the maxima of the dipole matrix element are correlated with large changes in the CB population. In Fig. 6(b) these changes are constructive resulting in large CB population after the pulse ends, while in Fig. 6(a) the changes are destructive, which results in small final CB population. Whether changes of the CB population are constructive or destructive is determined by the phase accumulated between two consecutive passages of point "2". The phase is determined by exponential factor in the expression (14) for the vector function $\mathbf{Q}_\mathbf{q}(t)$.

B. Transferred charge

A strong optical pulse applied to metal or dielectric causes transfer of charge parallel to the pulse field; the direction of the transfer (the sign of the transferred charge) is determined by the carrier-envelope phase (CEP) of the pulse [15,17,19]. In this article, the maximum of the carrier oscillation and its envelope coincide, which implies zero CEP (effect of the CEP on graphene high-field behavior will be considered elsewhere). In such a case, the transfer in dielectric occurs in the direction of the field maximum, and in metal in the opposite direction [15,19]. Below we show that graphene (a semimetal) is unique and different from both metals and insulators.

Given that the area of the pulse is zero, the transferred charge is entirely due to optical nonlinearity. Current density $\mathbf{j}$ and polarization $\mathbf{P}$ are exactly related, $\mathbf{j} = \dot{\mathbf{P}}$. The density of the net transferred charge per pulse, Q_{tr}, is thus determined by the residual polarization after the pulse end, $Q_{tr} = P_x^{(res)}$, where x is the direction of the field (charge transfer direction). Hence, in a single-pulse experiment, the charge transfer is strictly zero in the absence of relaxation (i.e., for adiabatic, reversible processes). Consequently, in graphene, where the strong-field processes are highly irreversible and the residual charges dominate, the charge transfer should be uniquely strong.

Formal expression for Q_{tr} is given in the SI; here in Fig. 7 we illustrate the results. Panel (a) displays temporal dynamics of the current. In the first half of the pulse, this current is negative, while in the second half it is positive where also significant relaxation is evident in a strong field, $F_0 = 2$ V/Å, case.

The total transferred charge per pulse, Q_{tr}, shown in Fig. 7(b), is positive (as for dielectrics [15]) for $F_0 \lesssim 1.5$ V/Å and negative for larger fields (i.e., the transfer occurs opposite to the direction of the maximum field, as for metals [19]); Q_{tr} rather weakly depends on doping.

The charge transfer per pulse in bulk silica (quartz) [15] is $Q_{tr} \sim 10^{-5}$ C/m^2 at $F_0 \approx 2$ V/Å. To compare with graphene, it should be multiplied by the thickness of the graphene monolayer, ∼0.1 nm, which yields for quartz an equivalent of $Q_{tr} \sim 10^{-15}$ C/m per atomic monolayer. Our present result is $Q_{tr} \gtrsim 10^{-9}$ C/m. Thus, in strong-field charge transfer, graphene is six orders of magnitude more efficient than quartz.

IV. CONCLUSION

To briefly summarize, we have shown that graphene subjected to an ultrafast (one optical oscillation) and strong (∼1 V/Å) optical pulse exhibits fundamental behavior

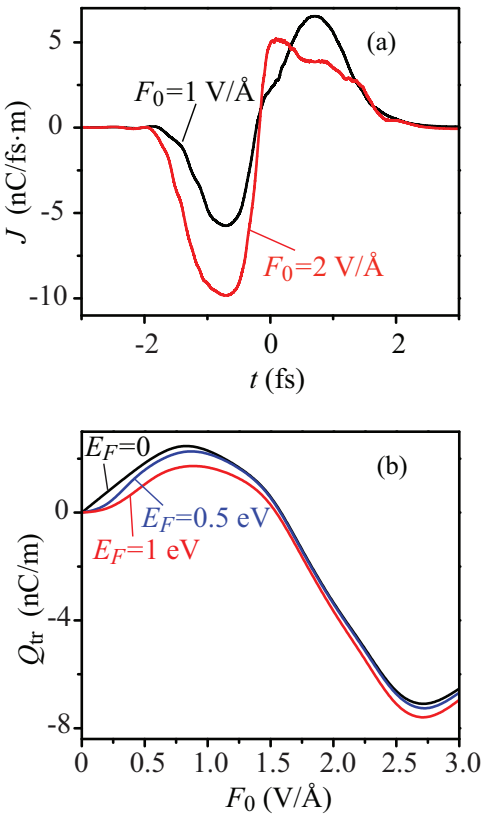

FIG. 7. (Color online) (a) Electric current density in graphene as a function of time for two amplitudes, $F_0 = 1.0$ V/Å and $F_0 = 2.0$ V/Å. (b) Transferred charge density through graphene monolayer as a function of F_0 for different levels of graphene doping (defined by electron Fermi energy E_F).

dramatically different from both insulators and metals. Field-induced, Zener-type VB $\leftrightarrow$ CB electron transfer is deeply irreversible (nonadiabatic): the residual (after-pulse) CB population is close to the maximum one. The reciprocal space (quasimomentum) dynamics is developing on a time scale $\sim$1 fs forming momentum distribution, which exhibits deep fringes with the population probability changing in the full interval between 1 and zero with the periodicity independent of the field amplitude. This unique periodic k distribution can be accessed experimentally.

In our calculations above we have described the interaction of optical pulse with graphene within coherent electron dynamics, assuming that the duration of the pulse is longer than the corresponding relaxation times. The relaxation times during ultrafast excitation of graphene have been investigated experimentally [25,27]. The carrier-carrier scattering in Ref. [25] is observed to occur during 30–140 fs. In Ref. [27], the observed electron-electron scattering kinetics unfolds on times 10 fs or longer. The field-induced processes that we predicted are extremely fast: the populations of the valence and conduction changes within subcycle intervals, on the time scale of 500 attoseconds or shorter. In our article, the superstrong near-single-oscillation pulse is not longer than 4 fs, which is shorter than experimentally observed scattering times, and it drives very significant changes in the electron distribution, which is also highly anisotropic.

The strong optical pulse causes the net charge transfer (per unit width of the graphene, per pulse) $Q_{tr} \sim 10^{-9}$ C/m, which corresponds to a fs pulse of electric current in the plane of graphene with peak density $j \sim 10^{16}$ A/m^2. The charge is transferred in the direction of the maximum field for moderate field amplitudes ($F_0 \lesssim 1.5$ V/Å) and opposite to that for high fields. This ultrafast charge transfer phenomenon is almost independent of graphene doping. The charge transfer in fused silica during propagation of fs optical pulse has been measured experimentally in Ref. [15]. Similar technique can be applied for graphene. The fs currents and charge transfer in graphene may provide a fundamental basis for detection and calibration of ultrashort intense laser pulses. They are promising for petahertz-bandwidth information processing.

ACKNOWLEDGMENTS

Major funding was provided by Grant No. DE-FG02-01ER15213 from the Chemical Sciences, Biosciences and Geosciences Division. Supplementary funding came from Grant No. DE-FG02-11ER46789 from the Materials Sciences and Engineering Division of the Office of the Basic Energy Sciences, Office of Science, U.S. Department of Energy, and NSF Grant No. ECCS-1308473. During MIS's Sabbaticals at Munich, this work was supported by the Max Planck Society and the Deutsche Forschungsgemeinschaft Cluster of Excellence: Munich Center for Advanced Photonics (http://www.munich-photonics.de).

[1] R. H. Fowler and L. Nordheim, Proc. R. Soc. A **119**, 173 (1928).
[2] C. Zener, Proc. R. Soc. A **145**, 523 (1934).
[3] L. V. Keldysh, J. Expt. Theor. Phys. **33**, 763 (1957) [Sov. Phys. JETP **6**, 994 (1958)].
[4] G. H. Wannier, Phys. Rev. **117**, 432 (1960).
[5] M. Lenzlinger and E. H. Snow, J. Appl. Phys. **40**, 278 (1969).
[6] M. Lenzner, J. Kruger, S. Sartania, Z. Cheng, C. Spielmann, G. Mourou, W. Kautek, and F. Krausz, Phys. Rev. Lett. **80**, 4076 (1998).
[7] L. Miaja-Avila, C. Lei, M. Aeschlimann, J. L. Gland, M. M. Murnane, H. C. Kapteyn, and G. Saathoff, Phys. Rev. Lett. **97**, 113604 (2006).
[8] M. I. Stockman, M. F. Kling, U. Kleineberg, and F. Krausz, Nat. Photon. **1**, 539 (2007).
[9] M. Durach, A. Rusina, M. F. Kling, and M. I. Stockman, Phys. Rev. Lett. **105**, 086803 (2010).
[10] M. Gertsvolf, M. Spanner, D. M. Rayner, and P. B. Corkum, J. Phys. B **43**, 131002 (2010).
[11] M. Durach, A. Rusina, M. F. Kling, and M. I. Stockman, Phys. Rev. Lett. **107**, 086602 (2011).
[12] S. Zherebtsov, T. Fennel, J. Plenge, E. Antonsson, I. Znakovskaya, A. Wirth, O. Herrwerth, F. Suessmann, C. Peltz, I. Ahmad *et al.*, Nat. Phys. **7**, 656 (2011).
[13] M. Kruger, M. Schenk, and P. Hommelhoff, Nature (London) **475**, 78 (2011).

[14] S. Ghimire, A. D. DiChiara, E. Sistrunk, P. Agostini, L. F. DiMauro, and D. A. Reis, Nat. Phys. **7**, 138 (2011).
[15] A. Schiffrin, T. Paasch-Colberg, N. Karpowicz, V. Apalkov, D. Gerster, S. Muhlbrandt, M. Korbman, J. Reichert, M. Schultze, S. Holzner *et al.*, Nature (London) **493**, 70 (2012).
[16] M. Schultze, E. M. Bothschafter, A. Sommer, S. Holzner, W. Schweinberger, M. Fiess, M. Hofstetter, R. Kienberger, V. Apalkov, V. S. Yakovlev *et al.*, Nature (London) **493**, 75 (2012).
[17] F. Krausz and M. I. Stockman, Nat. Photon. **8**, 205 (2014).
[18] A. V. Mitrofanov, A. J. Verhoef, E. E. Serebryannikov, J. Lumeau, L. Glebov, A. M. Zheltikov, and A. Baltuška, Phys. Rev. Lett. **106**, 147401 (2011).
[19] V. Apalkov and M. I. Stockman, Phys. Rev. B **88**, 245438 (2013).
[20] H. K. Kelardeh, V. Apalkov, and M. I. Stockman, Phys. Rev. B **90**, 085313 (2014).
[21] A. K. Geim and K. S. Novoselov, Nat. Mater. **6**, 183 (2007).
[22] A. H. C. Neto, F. Guinea, N. M. R. Peres, K. S. Novoselov, and A. K. Geim, Rev. Mod. Phys. **81**, 109 (2009).
[23] D. S. L. Abergel, V. Apalkov, J. Berashevich, K. Ziegler, and T. Chakraborty, Adv. Phys. **59**, 261 (2010).
[24] E. H. Hwang and S. Das Sarma, Phys. Rev. B **77**, 195412 (2008).
[25] M. Breusing, S. Kuehn, T. Winzer, E. Malic, F. Milde, N. Severin, J. P. Rabe, C. Ropers, A. Knorr, and T. Elsaesser, Phys. Rev. B **83**, 153410 (2011).
[26] E. Malic, T. Winzer, E. Bobkin, and A. Knorr, Phys. Rev. B **84**, 205406 (2011).
[27] D. Brida, A. Tomadin, C. Manzoni, Y. J. Kim, A. Lombardo, S. Milana, R. R. Nair, K. S. Novoselov, A. C. Ferrari, G. Cerullo *et al.*, Nat. Commun. **4**, 1987 (2013).
[28] I. Gierz, J. C. Petersen, M. Mitrano, C. Cacho, I. C. E. Turcu, E. Springate, A. Stöhr, A. Köhler, U. Starke, and A. Cavalleri, Nat. Mater. **12**, 1119 (2013).
[29] A. Tomadin, D. Brida, G. Cerullo, A. C. Ferrari, and M. Polini, Phys. Rev. B **88**, 035430 (2013).
[30] B. Y. Sun and M. W. Wu, New J. Phys. **15**, 083038 (2013).
[31] T. Oka and H. Aoki, Phys. Rev. B **79**, 081406 (2009).
[32] Z. H. Gu, H. A. Fertig, D. P. Arovas, and A. Auerbach, Phys. Rev. Lett. **107**, 216601 (2011).
[33] H. L. Calvo, H. M. Pastawski, S. Roche, and L. E. F. F. Torres, Appl. Phys. Lett. **98**, 232103 (2011).
[34] Y. H. Wang, H. Steinberg, P. Jarillo-Herrero, and N. Gedik, Science **342**, 453 (2013).
[35] P. R. Wallace, Phys. Rev. **71**, 622 (1947).
[36] J. C. Slonczewski and P. R. Weiss, Phys. Rev. **109**, 272 (1958).
[37] R. Saito, G. Dresselhaus, and M. Dresselhaus, *Physical Properties of Carbon Nanotubes* (Imperial College Press, London, 1998).
[38] S. Reich, C. Thomsen, and J. Maultzsch, *Carbon Nanotubes* (Wiley-VCH, Weinheim, 2004).
[39] W. V. Houston, Phys. Rev. **57**, 184 (1940).
[40] L. D. Landau and E. M. Lifshitz, *Quantum Mechanics: Non-Relativistic Theory* (Pergamon Press, Oxford and New York, 1965).
[41] J. Jung and A. H. MacDonald, Phys. Rev. B **87**, 195450 (2013).
[42] V. Apalkov and M. I. Stockman, Phys. Rev. B **86**, 165118 (2012).
[43] Y. B. Zhang, Y. W. Tan, H. L. Stormer, and P. Kim, Nature (London) **438**, 201 (2005).
[44] M. Jablan, H. Buljan, and M. Soljacic, Phys. Rev. B **80**, 245435 (2009).
[45] S. Kim, I. Jo, D. C. Dillen, D. A. Ferrer, B. Fallahazad, Z. Yao, S. K. Banerjee, and E. Tutuc, Phys. Rev. Lett. **108**, 116404 (2012).
[46] F. Sussmann, S. Zherebtsov, J. Plenge, N. G. Johnson, M. Kubel, A. M. Sayler, V. Mondes, C. Graf, E. Ruhl, G. G. Paulus *et al.*, Rev. Sci. Instrum. **82**, 093109 (2011).